Supplementary Information for

A two photon tandem photoanode with black phosphorus quantum dot sensitized BiVO$_4$ for solar water splitting

Bingjun Jin,‡[a,b,g] Yoonjun Cho,‡[b] Cheolwoo Park,[c] Jeehun Jeong,[d] Sungsoon Kim,[b] Jie Jin,[b] Wooyul Kim,[c] Luyang Wang,[d] Siyu Lu,[e] Shengli Zhang,[a] Sang Ho Oh,[d] Kan Zhang,*[a,b] and Jong Hyeok Park*[b]

Affiliations:

[a] MIIT Key Laboratory of Advanced Display Materials and Devices, Institute of Optoelectronics and Nanomaterials, School of Materials Science and Engineering, Nanjing University of Science and Technology, Nanjing 210094, P. R. China.

[b] Department of Chemical and Biomolecular Engineering, Yonsei University, 50 Yonsei-ro, Seodaemun-gu, Seoul 03722, Republic of Korea.

[c] Department of Chemical and Biological Engineering, Sookmyung Women's University, Seoul 04310, Republic of Korea.

[d] College of New Materials and New Energies, Shenzhen Technology University, Shenzhen, Guangdong 518118, P. R. China.

[e] Green Catalysis Center, and College of Chemistry, Zhengzhou University, Zhengzhou, 450000 P. R. China

[g]† Current address: School of Applied Physics and Materials, Wuyi University, Jiangmen 529020, P. R. China

AUTHOR INFORMATION
‡ These authors contributed equally: Bingjun Jin, and Yoonjun Cho

Corresponding Author
*E-mail: zhangkan@njust.edu.cn (Kan Zhang); lutts@yonsei.ac.kr (Jong Hyeok Park)

METHODS

Materials. All chemicals were of analytical grade and used directly without any further purification. Deionized water with resistivity of 18.25 MΩ.cm was used in all reactions. Fluorine-doped tin oxide (FTO, TEC-8, Pilkilton) glass was cleaned in ethanol, acetone and distilled water by sonication for 10 min respectively. Then, the FTO glass was dipped in a miscible liquid of sulfuric acid and hydrogen peroxide (7:3 by vol%) for another 10 min in order to make the glass hydrophilic. BP powder was s purchased from Mukenano Co. LTD.

Preparation of black phosphorus quantum dots (BPQDs). BP powder (0.5 g) was added to 150 mL of isopropanol (IPA), and argon was pumped through the solution for 10 mins to remove the oxygen in the isopropanol. Then, ultrasonic treatment @100 W was carried out for 10 h. After that, the obtained dispersion was transferred to an iron cup for a new round of ultrasonic treatment (@800 W for 2 h); meanwhile, argon was continuously pumped through the dispersion to protect the BP from oxidation.

Preparation of photoetched $BiVO_4$ photoanode (E-$BiVO_4$). $BiVO_4$ photoanode was prepared by a three-step process via a modified method as reported by Choi's group.[6] Firstly, BiOI nanosheets film on FTO glass with the area of 4.0 cm^2 was fabricated by the electrochemical deposition method. Then the as-prepared brown color BiOI film was converted to $BiVO_4$ by annealing method with annealing in air at 450 °C (ramping rate = 2 °C per min) for 2 h. After that, the excess V_2O_5 was removed by soaking the as-prepared $BiVO_4$ electrode in 1 M NaOH solution for 30 min with continuous stirring. Lastly, the pure $BiVO_4$ electrode was collected by washing with deionized water for several times and dried at RT. Then the $BiVO_4$ photoanode was immersed in 1 M KBi buffer solution containing 0.2 M Na_2SO_3 with simulated AM 1.5 G illumination and etched for 10 min.

Preparation of E-$BiVO_4$/BPQDs/OL-OEC photoanode. Firstly, the E-$BiVO_4$/BPQDs photoanode was prepared as follows. The obtained $BiVO_4$ photoanode was placed on a platform horizontally in order to make the BPQDs cover it uniformly. 200 μL of the as-prepared BPQDs solution (in IPA) was dropped on the surface of $BiVO_4$ photoanode, and then kept in a petri dish until the sample became dry naturally. Different amounts of BPQDs loading was depended on the repeat times of the dropping process. The above preparation process was carried out in the glove box in order to avoid the oxidation of BPQDs. Then amorphous TiO_2

overlayer was deposited on the surface of BiVO$_4$/BPQDs photoanode by a modified electrodeposition method. Briefly, TiCl$_3$ solution was prepared by diluting 12% TiCl$_3$ solution (Aldrich) in HCl/DI water solution (total volume 21 mL with a ratio of 1:20). Then the pH of the solution was neutralized to 2.45 by adding 0.6 M NaHCO$_3$ solution slowly. The final solution is a Ti^{3+}-containing solution with Ti concentration is about 15 mM. The solution was purged with nitrogen for 30 min before electrodeposition, and then the as-prepared photoanode was immersed in the Ti^{3+}-containing solution by applying 0.02 V *vs.* SCE, which was carried out by chronoamperometry for 10-60 seconds. Lastly, the NiOOH OEC layer was synthesized using a simple photoassisted electrodeposition method.[1] The solution was purged with argon gas for 30 min before deposition, and a three electrodes system was used with Pt wire as the counter electrode, Ag/AgCl as the reference electrode, and the photoanode as the working electrode. The NiOOH layer was photoelectrodeposited in 0.1 M NiSO$_4$ solution at 0.11 V *vs.* Ag/AgCl for 5 min and followed with electrodeposition at 1.2 V *vs.* Ag/AgCl for 1 min. The E-BiVO$_4$/OL and E-BiVO$_4$/OL-OEC photoanodes were prepared by a similar procedure without BPQDs loading.

Material Characterization. The morphologies and structures of the samples were observed by field emission scanning electron microscopy (FESEM, JSM-7000F, Japan). Transmission electron microscopy (TEM) and high-resolution transmission electron microscopy (HRTEM) measurements were performed using a JEOL JEM-2100F (Japan) electron microscope. The EELS plasmon map was reconstructed by low-loss energy ranging from 6 to 40 eV. The crystalline structures were identified by X-ray diffraction (XRD) using a Siemens D500/5000 diffractometer in a Bragg–Brentano geometry under Cu Kα radiation at 40 keV and 40 mA. X-ray photoelectron spectroscopy (XPS) data were obtained from a SESXPS instrument (ESCA2000, VG Microtech, England). The AFM was measured by using Bruker Multimodel-8 equipment. UV-vis absorption spectra were obtained using a UV-vis spectrophotometer (Neosys-2000, Scinco Co. Ltd, Korea). EPR spectra were recorded at room temperature with an EPR spectrometer (Bruker, a320) at 77K. UPS spectra were collected on an Auger electron spectrometer (Thermofisher escalab 250xi), using a He I (21.22 eV) excitation line. PL was taken on Edinburgh FLS1000 equipped with an Oxford cryostat designed for optical measurement at 77 K.

Calculation methods. The DFT calculations are presented by using the generalized gradient approximation (GGA) with the Perdew–Burke–Ernzerhof (PBE) exchange–correlation

functional in the Vienna ab initio simulation package (VASP).[2, 3] The plane-wave cut-off energy is 500 eV and the vacuum thickness between two adjacent systems is larger than 15 Å. For the 2D black phosphorene, we use the Monkhorst–Pack k-points of 10×6×1 and the convergence criteria for the energy and the force in each direction are 10^{-5} eV and 0.005 eV/Å, respectively. For the black phosphorous quantum dots, the 1×1×1 Monkhorst–Pack k-points were adopted and the convergence criteria for the energy and the force in each direction are 10^{-3} eV and 0.01 eV/Å, respectively. For the black phosphorene, we use the Monkhorst–Pack k-points of 10×6×1 and the energy and the force convergence criteria are 10^{-5} eV and 0.005 eV/Å, respectively. The dispersion correction is also considered through Grimme's D2 method for multilayer systems in optimizing the system geometry.[4] The screened hybrid functional (HSE06) is also used to evaluate the band structures of monolayer and multilayer black phosphorene, which generally provides a more accurate description of the band gaps.[5]

Photoelectrochemical analysis. PEC measurements were performed in a 3-electrode system using an electrochemical workstation (CH Instrument, CHI 660) with the as-prepared photoanodes as working electrodes, Ag/AgCl (3 M NaCl) as reference electrode and Pt as the counter electrode. 0.5 M potassium phosphate buffer solution (KPi, pH=7.0) served as the electrolyte. All the samples were measured in the electrolyte treated with silver paste painted on the top to increase the conductivity, and a quartz cell with an aperture was used to determine the contact area between the samples and the electrolyte. The as-prepared photoelectrodes were illuminated from the back side by a solar simulator (Peccell, Yokohama, Japan, PEC-L01) equipped with an AM 1.5 G filter (100 mW cm^{-2}). Linear sweep voltammograms were measured under a bias voltage with a scan rate of 0.1 Vs^{-1}. Amperometric I–t curves was tested at a given bias voltage (*vs*. RHE). The Mott-Schottky plots were measured in a 0.5 M KPi containing 0.2 M Na_2SO_3 at a frequency of 1000 Hz under dark condition. The incident photon-to-current conversion efficiency (IPCE) was detected by using a monochromator (Polaronix K3100 IPCE Measurement System, McScience). The water splitting reactions were performed using an electrochemical work station with an applied bias voltage of 1.23 V (*vs*. RHE), and nitrogen gas was purged for 30 min to ensure the removal of dissolved oxygen. The generated gas was tested every 30 min by a commercial online automatic testing system (Perfectlight Sci&Tech Co., Ltd., Labsolar-6A) that was connected with a gas chromatography system (PerkinElmer, Clarus 580, USA, TCD, 5 Å molecular sieve columns and Ar carrier).

Table S1. The energy levels and the corresponding frontier molecular orbitals for different sizes of BPQDs (The nonperiodic boundary is terminated by H atoms).

		PBE		
	Diameter	HOMO	LUMO	Gap
$H_{12}P_{20}$	0.87 nm	-4.799	-2.396	2.403
$H_{16}P_{42}$	1.32 nm	-4.716	-2.743	1.973
$H_{22}P_{80}$	1.66 nm	-4.492	-2.885	1.607
$H_{30}P_{126}$	1.98 nm	-4.341	-2.934	1.407
$H_{32}P_{158}$	2.27 nm	-4.220	-2.841	1.379
$H_{40}P_{190}$	2.45 nm	-3.814	-2.546	1.268
$H_{40}P_{242}$	2.96 nm	-3.533	-2.338	1.195
$H_{46}P_{328}$	3.65 nm	-3.535	-2.400	1.135

Table S2. Summary of merits for the photocurrent density of $BiVO_4$ over 5.0 mA cm^{-2}.

Photoanode	Co-catalyst	performance	Lightspot	Ref.
Helix-WO$_3$/(W, Mo)-BiVO$_4$	FeOOH/NiOOH	5.35 mA cm^{-2} @ 1.23 vs. RHE in 0.5 M K$_2$SO$_4$ + KPi (pH 7)	Boosting charge separation by heterojunction interface with enhanced optical absorption	6
WO$_3$ nanowire/BiVO$_4$	Co–Pi	6.8 mA cm^{-2} @ 1.23 vs. RHE in 0.1 M KPi (pH 7)		7
Sb:SnO$_2$ nanowire/ BiVO$_4$	FeOOH/NiOOH	5.3 mA cm^{-2} @ 1.23 vs. RHE in 0.5 M KPi (pH 7)		8
Mo-BiVO$_4$/ B-C$_3$N$_4$	NiFeO$_x$	5.93 mA cm^{-2} @ 1.23 vs. RHE in PPB solution (pH 7)		9
Mo-BiVO$_4$/La:BaSnO$_3$	None	5.15 mA cm^{-2} @ 1.23 vs. RHE in 0.5 M KPi (pH 7)		10
N-BiVO$_4$	FeOOH/NiOOH	~5.0 mA cm^{-2} @ 1.23 vs. RHE in 0.5 M KPi (pH 7.2)	Extending optical absorption region of BiVO$_4$ with enhanced charge separation	11
H, 1% Mo:BiVO$_4$	FeOOH/NiOOH	~5.0 mA cm^{-2} @ 1.23 vs. RHE in 0.5 M KCi (pH 9.2)		12
[001]-oriented BiVO$_4$	Co–Pi	6.1 mA cm^{-2} @ 1.23 vs. RHE in 0.5 M KPi (pH 7)	Enhancing charge separation	13
BiVO$_4$	CoF$_2$	5.1 mA cm^{-2} @ 1.23 vs. RHE in 0.5 M KPi (pH 7)	Accelerating water oxidation kinetics with enhanced charge separation	14
BiVO$_4$	Molecular Co$_4$O$_4$ Cubane	~5.0 mA cm^{-2} @ 1.23 vs. RHE in 0.5 M borate buffer (pH 9.3)		15
BiVO$_4$/Carbon QDs	NiOOH/FeOOH	5.99 mA cm^{-2} @ 1.23 vs. RHE in 0.5 M KH$_2$PO$_4$ (pH 7)	Expanding optical absorption	16
Zn-BiVO$_4$/Graphene QDs	Co-Pi	5.03 mA cm^{-2} @ 1.23 vs. RHE in 0.1 M KPi (pH 7)		17
E-BiVO$_4$/BPQDs/TiO$_2$	NiOOH	6.2 mA cm^{-2} @ 1.23 vs. RHE in 0.5 M KPi (pH 7)	Expanding optical absorption with suppressed surface recombination	Our work

Description: In addition to enhanced charge separation, extended light harvesting and accelerated water oxidation kinetics, the surface charge recombination was successfully suppressed by TiO$_2$ passivation layer in our case. Although co-catalyst loading can hinder the surface charge recombination to some extent, the direct loading of co-catalyst on photoelectrode could not fully address the surface charge recombination issue.[18,19]
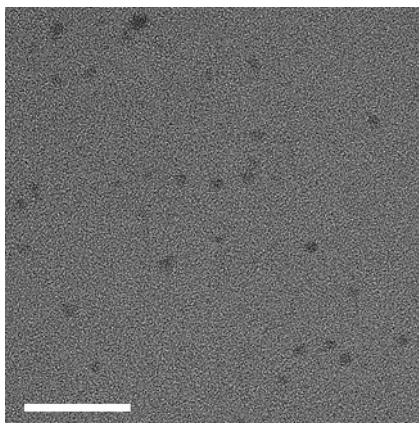
Fig. S1. TEM image of BPQDs, scan bar: 50 nm.
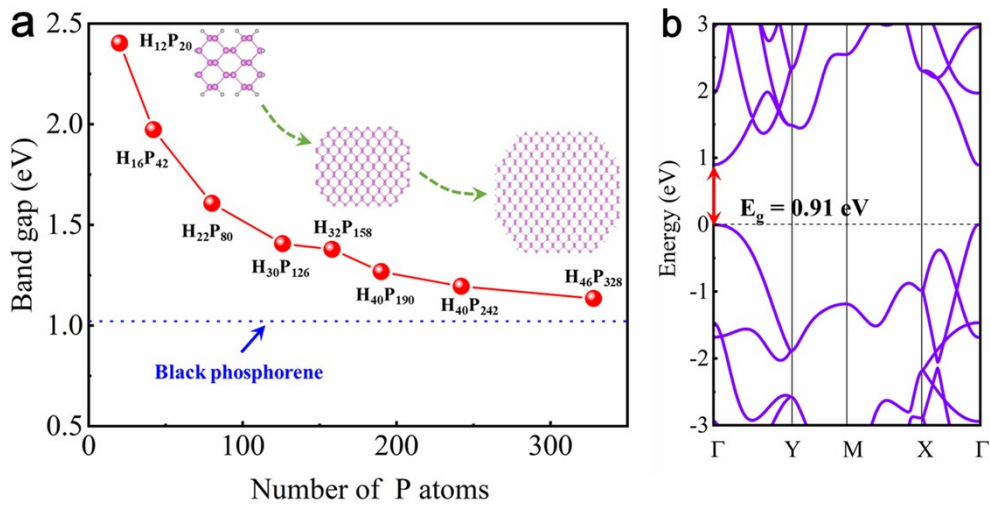
Fig. S2. (a) The bandgap changes as a function of P atom numbers; (b) Band structure of monolayered BP. All values are obtained by using PBE calculation method.
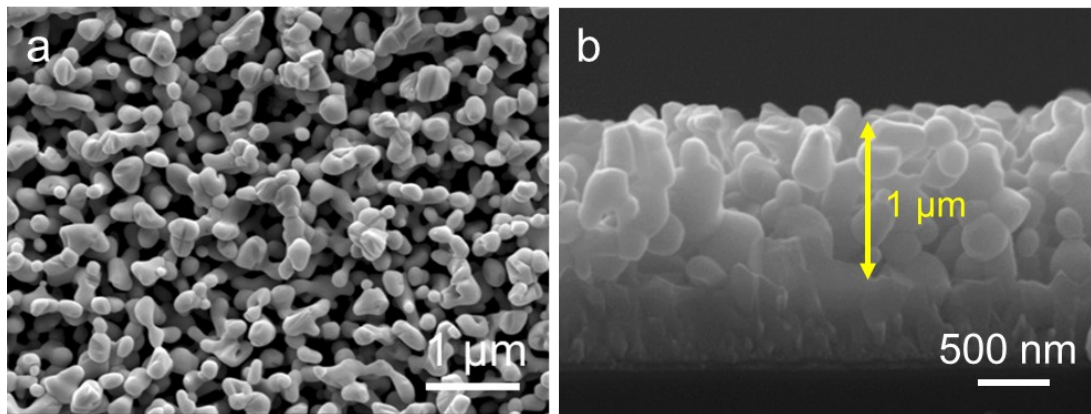
Fig. S3. Top and section view of the nanoporous $BiVO_4$ photoanode.
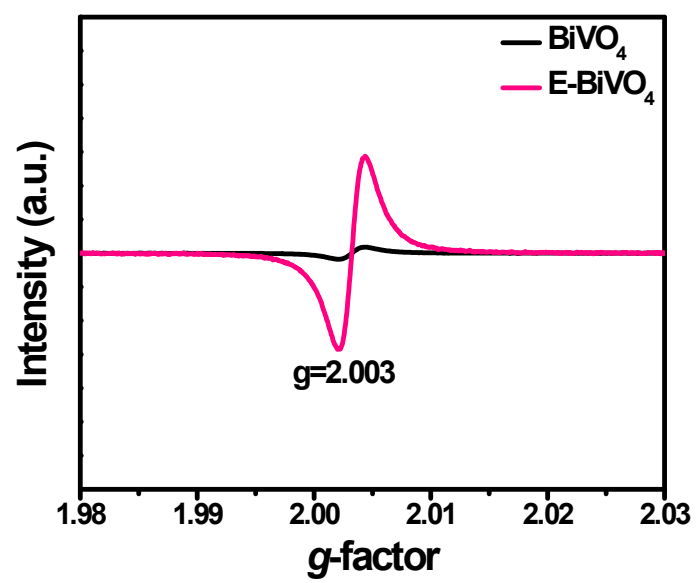
Fig. S4. Low-temperature (77K) EPR spectra of $BiVO_4$ and E-$BiVO_4$ photoanodes.
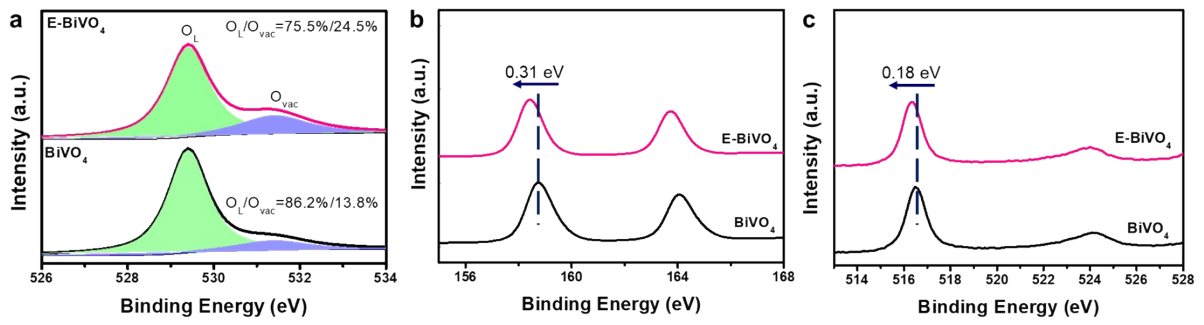
Fig. S5. XPS spectra of $BiVO_4$ and E-$BiVO_4$ photoanodes. (a) O1s, (b) Bi 4f and (c) V 2p.

Description:

In Fig. S5a, the peak at lower binding energy (~529.41 eV) is assigned to the lattice oxygen (O_L), while the peak at higher binding (~531.39 eV) energy can be ascribed to oxygen vacancies (O_{vac}).[20]
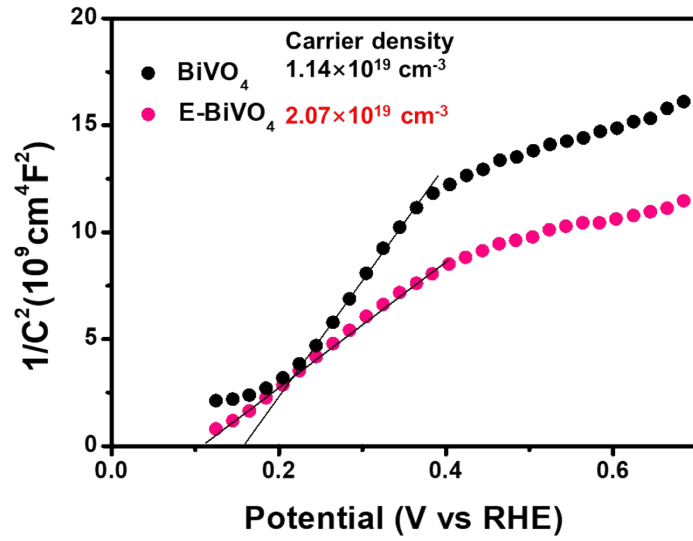
Fig. S6. Mott–Schottky plots of $BiVO_4$ and E-$BiVO_4$ photoanodes.

Description:

The carrier density can be calculated using Equation 1:[21]

$$N_d = 2\, q\varepsilon\varepsilon 0\, [d(1/c^2)/dV]^{-1}$$

Where the Nd is carrier density, q is the electron charge (1.60×10^{-19} C), ε is the dielectric constant of semiconductor (68 for $BiVO_4$), ε_0 is the permittivity of vacuum (8.854×10^{-14} F·cm^{-1}), $d(1/c^2)/dV$ is the slope of Mott-Schottky plot.
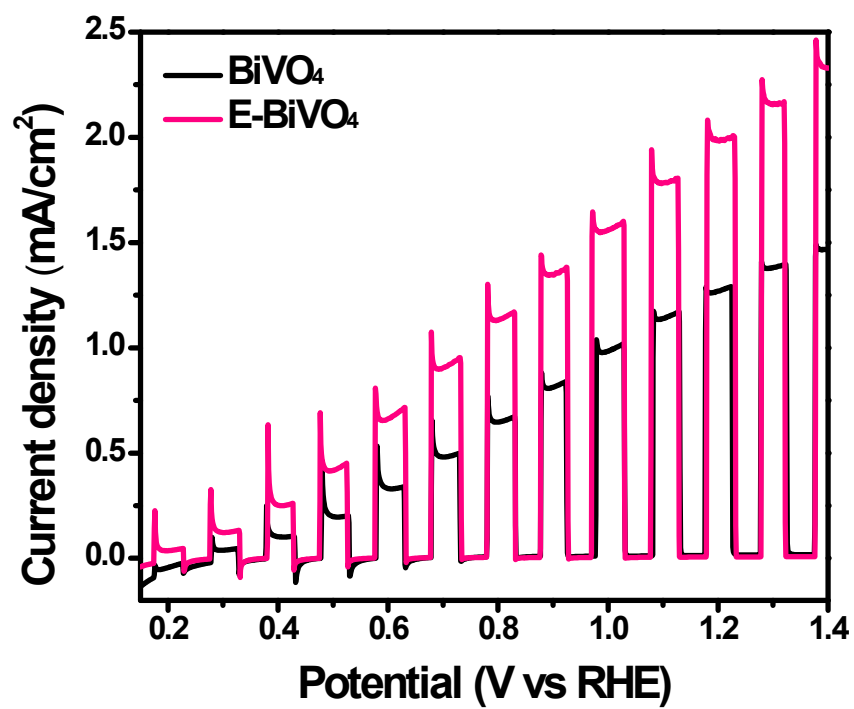
Fig. S7. Chopped *J-V* curves of BiVO$_4$ and E-BiVO$_4$ measured in KPi under AM 1.5 illumination.
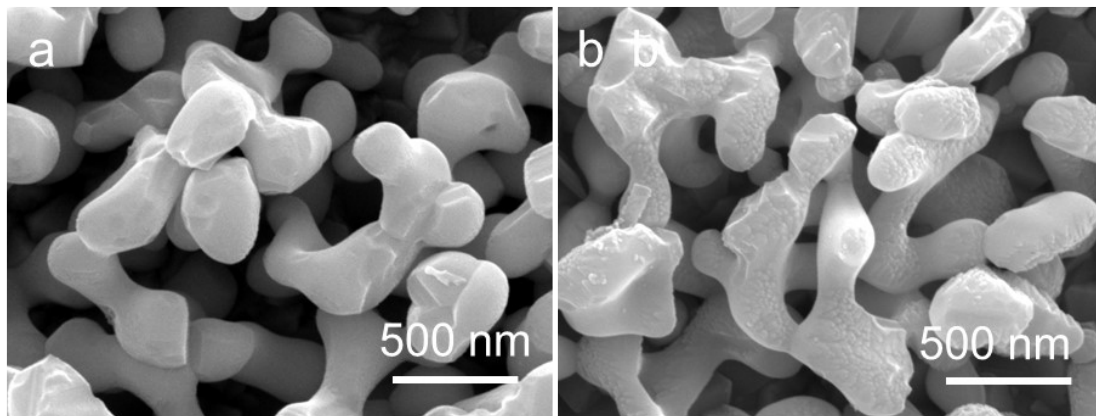
Fig. S8. SEM images of the BiVO$_4$/BPQDs (a) and E-BiVO$_4$/BPQDs (b) photoanode.
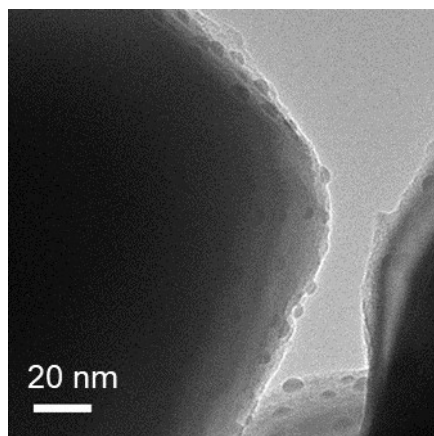
Fig. S9. TEM image of the BiVO$_4$/BPQDs photoanode.
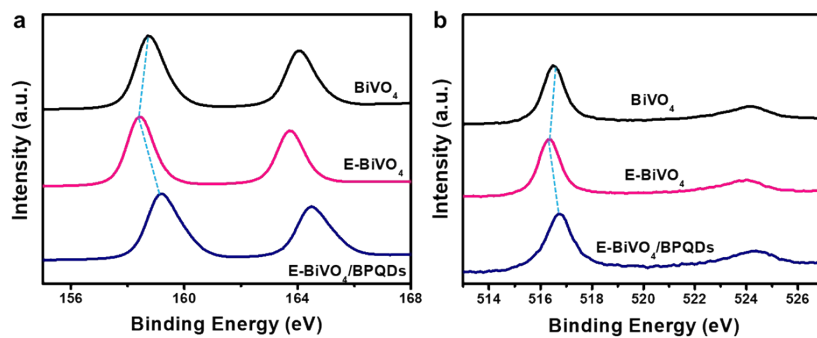
Fig. S10. Comparison of (a) Bi 4f and (b) V 2p XPS spectra of BiVO$_4$, E-BiVO$_4$ and E-BiVO$_4$/BPQDs photoanodes.
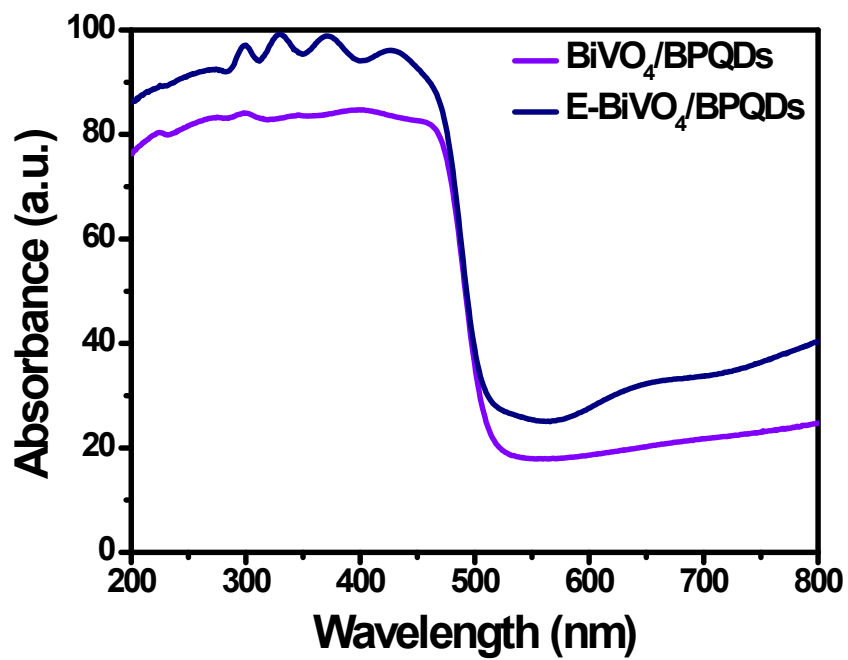
Fig. S11. UV-vis-NIR absorption spectra of $BiVO_4$-BPQDs and E-$BiVO_4$/BPQDs.
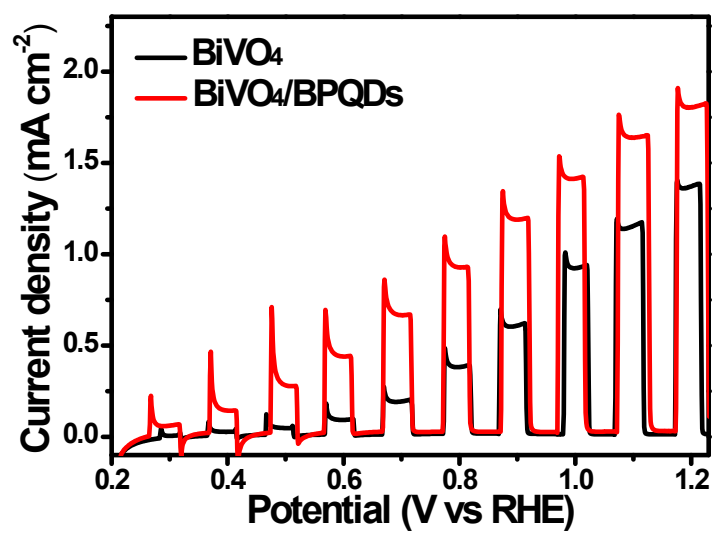
Fig. S12. Chopped *J-V* curves of $BiVO_4$ and $BiVO_4$/BPQDs measured in KPi under AM 1.5 illumination.
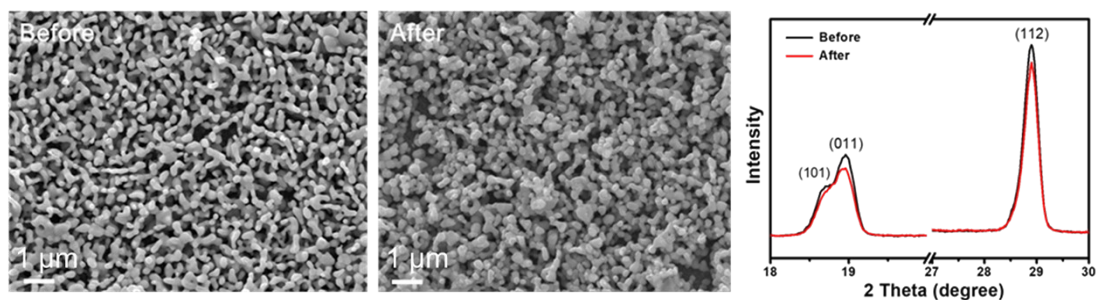
Fig. S13. SEM and XRD of BiVO$_4$ photoanode before and after long-term stability test.

Description:

The photo-corrosion of BiVO$_4$ was investigated by comparing SEM images and XRD patterns before and after long-term stability testing. It's clearly that the obviously changed morphology and the decrease in intensity of the major Bragg peaks of BiVO$_4$ are clear indication that chemical dissolution of pure BiVO$_4$ photoanode had occurred after stability test.
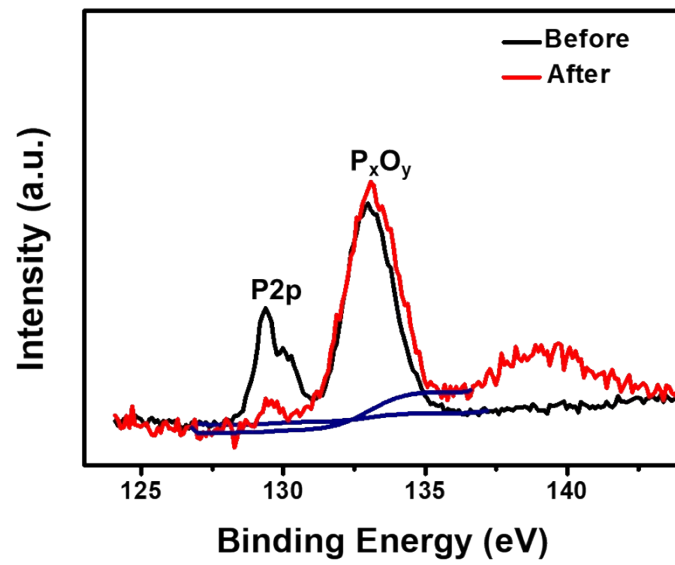
Fig. S14. P2p XPS spectrum of BiVO$_4$/BPQDs photoanodes before and after long time testing. A disappeared P 2p peak indicates the easier oxidation of BPQDs during photoelectrochemical water splitting.
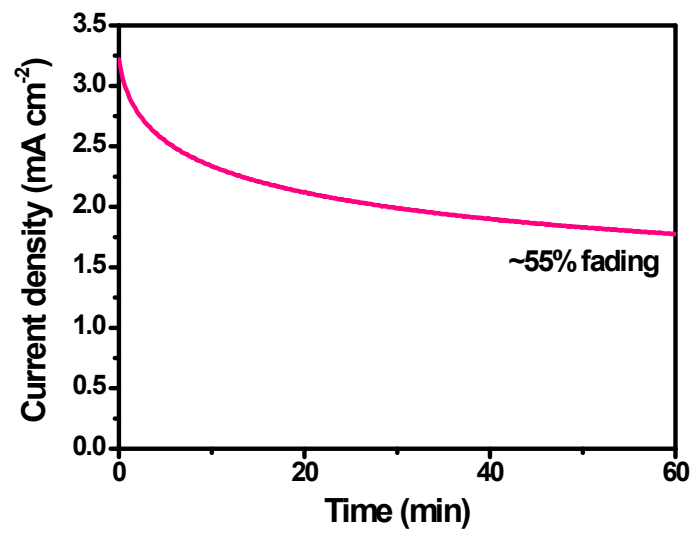
Fig. S15. Photocurrent density stability of E-BiVO$_4$/BPQDs photoanode at 1.23 V vs. RHE.
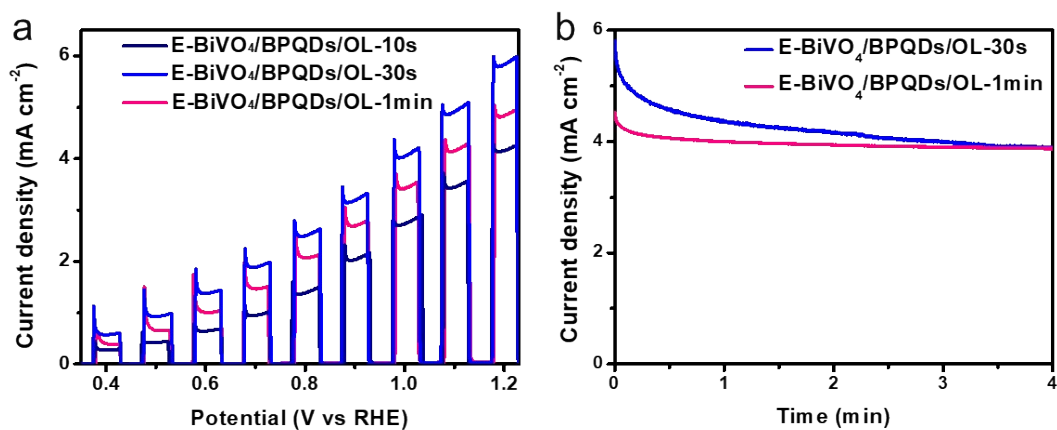
Fig. S16. (a) Chopped *J–V* curves of E-BiVO₄/BPQDs photoanode with different electrodeposition time of TiO₂ OL and (b) stability testing of E-BiVO₄/BPQDs with 30 seconds and 1 min electrodeposition time of TiO₂ OL measured in KPi electrolyte under AM 1.5 illumination.
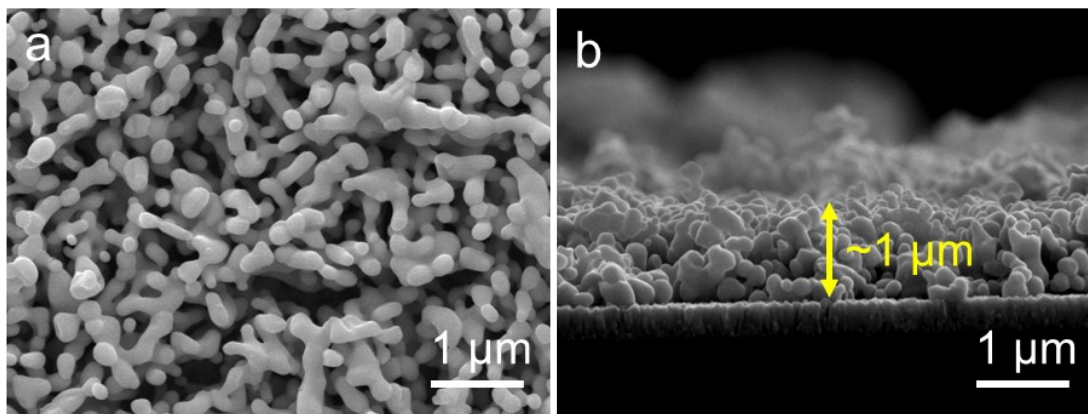
Fig. S17. Top and section view of E-BiVO$_4$/BPQDs/OL with 1min electrodeposition time.
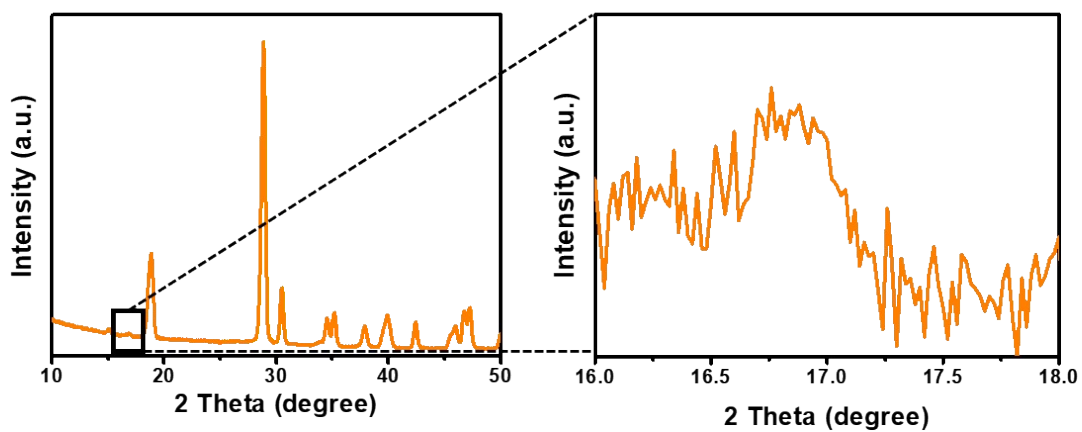
Fig. S18. XRD data of the E-BiVO$_4$/BPQDs/OL with 1min electrodeposition time.
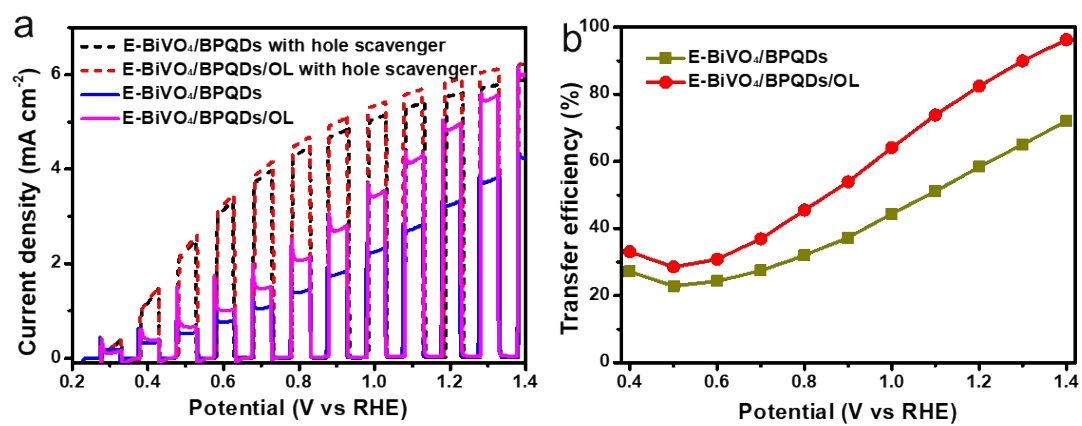
Fig. S19. (a) chopped *J-V* curves of E-BiVO$_4$/BPQDs and E-BiVO$_4$/BPQD/OL with/without hole scavenger. (b) charge transfer efficiencies calculated from Supplementary Figure 19a.
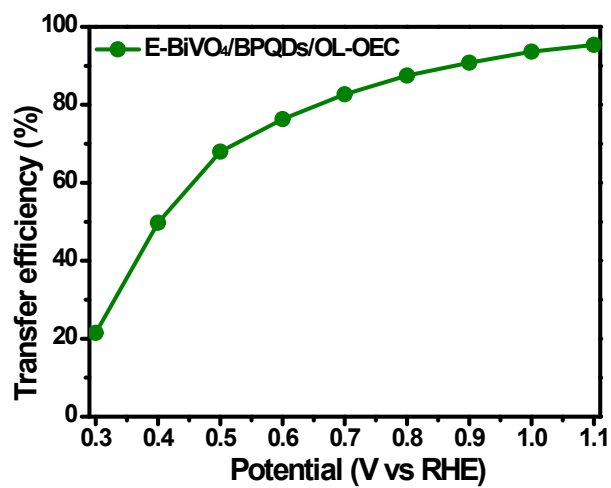
Fig. S20. Charge transfer efficiency of E-BiVO$_4$/BPQDs/OL-OEC calculated from Supplementary Figure 4b.
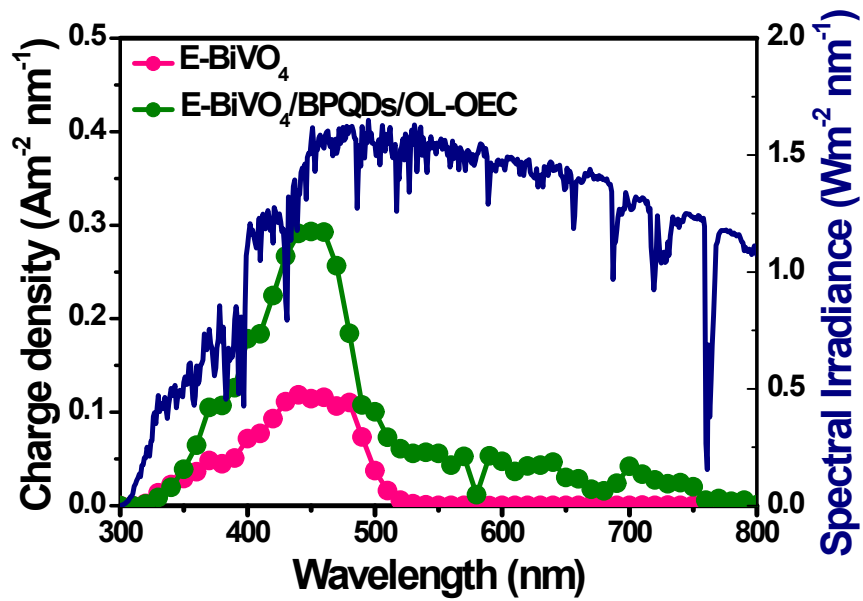
Fig. S21. Charge density of E-BiVO$_4$/BPQDs/OL-OEC calculated by IPCE result against the solar spectrum.
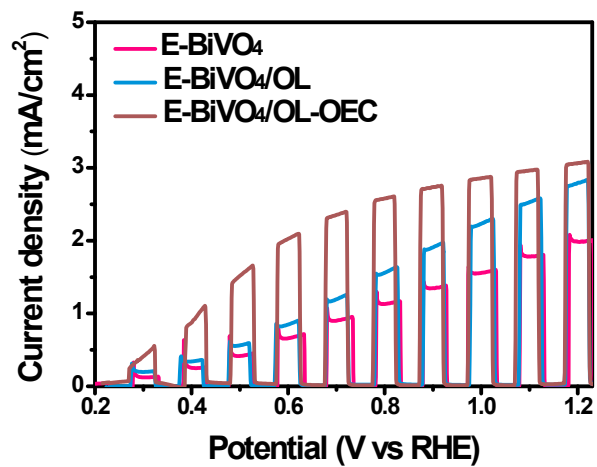
Fig. S21. Chopped *J-V* curves of E-BiVO$_4$/OL and E-BiVO$_4$/OL-OEC.
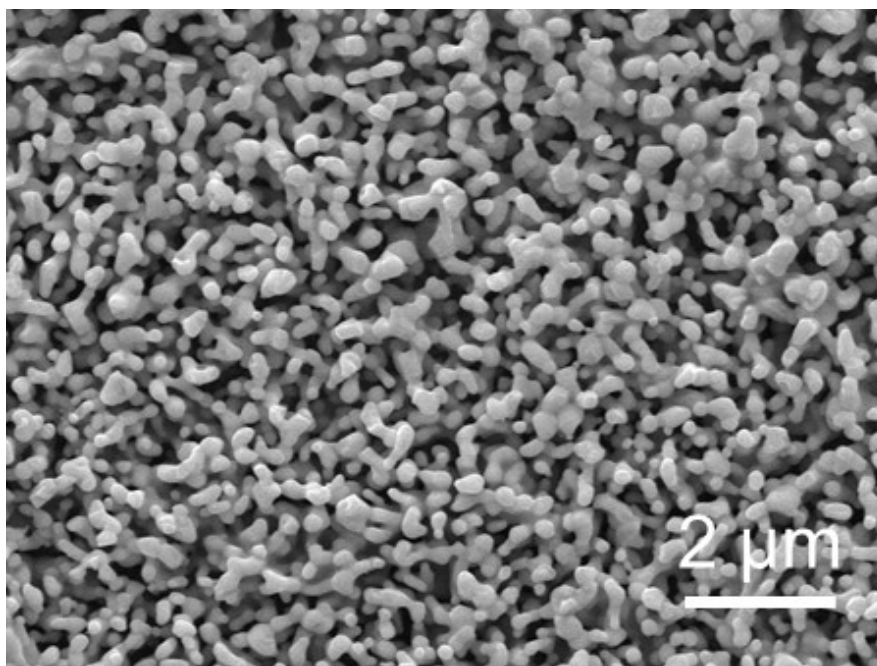
Fig. S23. SEM image of the E-BiVO$_4$/BPQDs/OL-OEC photoanode after long-term stability testing, scan bar: 100 nm.
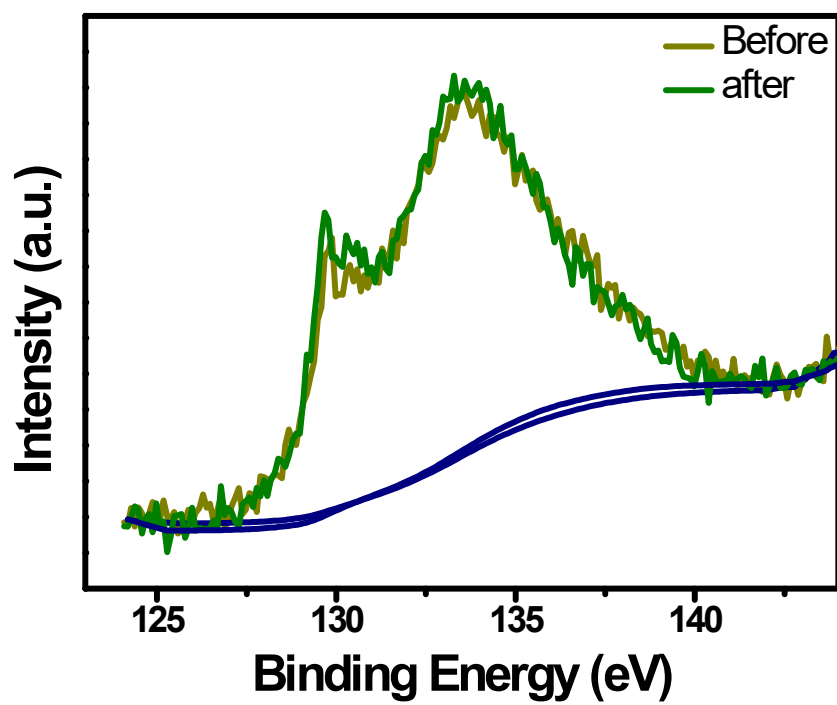
Fig. S24. High-resolution XPS spectra of P 2p for the E-BiVO$_4$/BPQDs/OL-OEC photoanode after long-term stability testing.
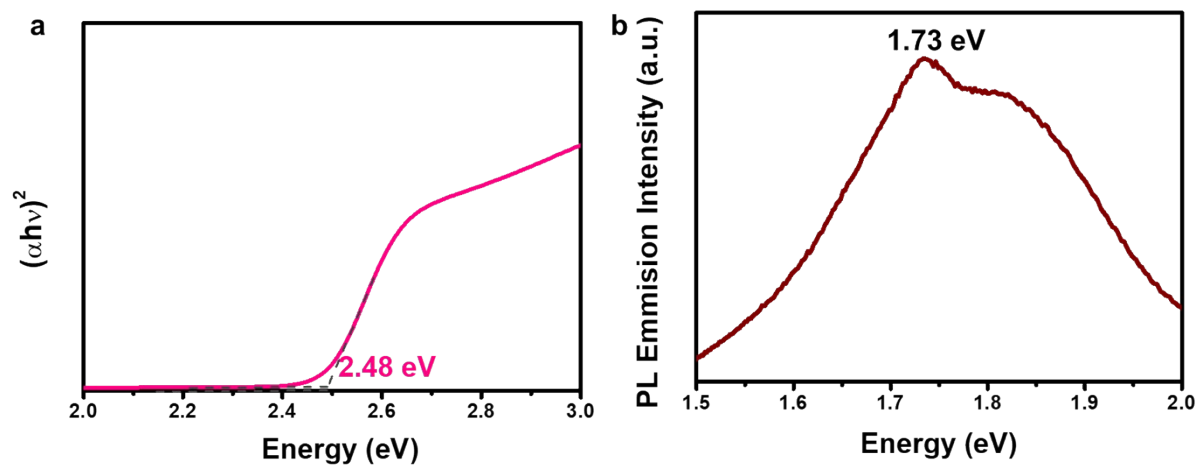
Fig. S25. (a) The plot of transformed Kubelka–Munk function versus the energy of light. (b) Emission steady-state PL spectrum of BPQDs powder at 77 K.
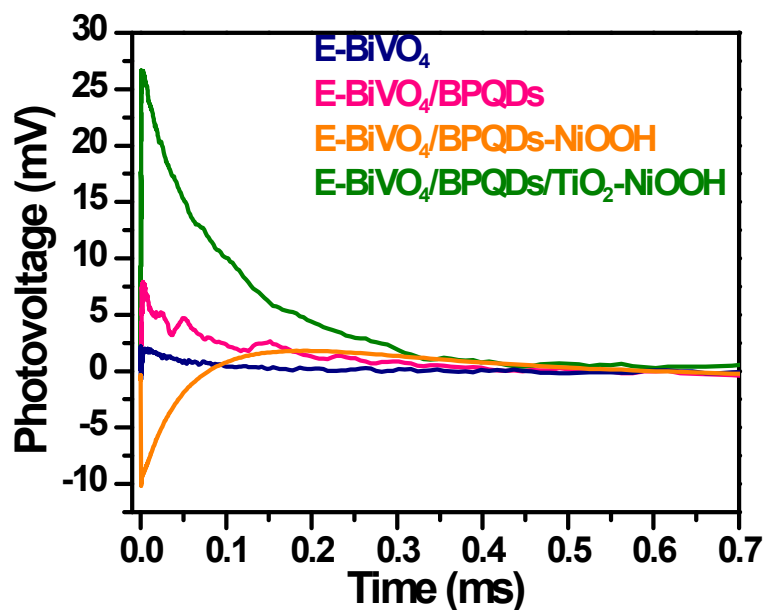
Fig. S26. TS-SPV responses of E-BiVO$_4$, E-BiVO$_4$/BPQDs, E-BiVO$_4$/BPQDs-NiOOH and E-BiVO$_4$/BPQDs/TiO$_2$-NiOOH photoanodes. The wavelength and intensity of the excitation pulse are 355 nm and 50 μJ, respectively.

Description:

Generally, the N-type semiconducting E-BiVO$_4$ photoanode, having upward band bending, exhibits a positive photovoltage response due to surface-reaching holes.[22] It can be seen that the photovoltage response of E-BiVO$_4$/BPQDs/TiO$_2$-NiOOH is dramatically enhanced compared with that of E-BiVO$_4$ or E-BiVO$_4$/BPQDs, indicating that the surface-reaching holes are efficiently promoted.

SUPPORTING REFERENCES

1. K. Zhang, B. Jin, C. Park, Y. Cho, X. Song, X. Shi, S. Zhang, W. Kim, H. Zeng, and J. H. Park, *Nat. Commun.* 2019, **10**, 2001.

2. G. Kresse, and J. Furthmüller, *Phys. Rev. B* 1996, **54**, 11169-11186.

3. J. P. Perdew, K. Burke, and M. Ernzerhof, *Phys. Rev. Lett.* 1996, **77**, 3865-3868.

4. S. Grimme, S. Ehrlich, and L. Goerigk, *J. Comput. Chem.* 2011, **32**, 1456-1465.

5. J. Heyd. G. E. Scuseria, and M. Ernzerhof, *J. Chem. Phys.* 2003, **118**, 8207-8215.

6. X. Shi, I. Y. Choi, K. Zhang, J. Kwon, D. Y. Kim, J. K. Lee, S. H. Oh, J. K. Kim, and J. H. Park, *Nat. Commun.* 2014, **5**, 1-8.

7. Y. Pihosh, I. Turkevych, K. Mawatari, J. Uemura, Y. Kazoe, S. Kosar, K. Makita, T. Sugaya, T. Matsui, D. Fujita, M. Tosa, M. Kondo, and T. Kitamori, *Sci. Rep.* 2015, **5**, 11141.

8. L. Zhou, C. Zhao, B. Giri, P. Allen, X. Xu, H. Joshi, Y. Fan, L. V. Titova, and P. M. Rao, *Nano Lett.* 2016, **16**, 3463-3474.

9. K. -H. Ye, H. Li, D. Huang, S. Xiao, W. Qiu, M. Li, Y. Hu, W. Mai, H. Ji, and S. Yang, *Nat. Commun.* 2019, **10**, 1-9.

10. J. Jian, Y. Xu, X. Yang, W. Liu, M. Fu, H. Yu, F. Xu, F. Feng, L. Jia, D. Friedrich, R. Van de Krol, and H. Wang, *Nat. Commun.* 2019, **10**, 1-9.

11. K. T. Woo, P. Yuan, G. Galli, and K. -S. Choi, *Nat. Commun.* 2015, **6**, 1-10.

12. J. H. Kim, J. -W. Jang, Y. H. Jo, F. F. Abdi, Y. H. Lee, R. van de Krol, and J. S. Lee, *Nat. Commun.* 2016, **7**, 1-9.

13. H. S. Han, S. Shin, D. H. Kim, I. J. Park, J. S. Kim, P. -S. Huang, J. -K. Lee, I. S. Cho, and X. Zheng, X. *Energy Environ. Sci.* 2018, **11**, 1299-1306.

14. B. Zhang, L. Chou, and Y. Bi, *App. Catal. B-Environ.* 2020, **262**, 118267.

15. Y. Wang, F. Li, X. Zhou, F. Yu, J. Du, L. Bai, and L. Sun, *Angew. Chem. Int. Ed.* 2017, **56**, 6911-6915.

16. K. -H. Ye, Z. Wang, J. Gu, S. Xiao, Y. Yuan, Y. Zhu, Y. Zhang, W. Mai, and S. Yang. *Energy Environ. Sci.* 2017, **10**, 772-779.

17. Q. Pan, K. Yang, G. Wang, D. Li, J. Sun, B. Yang, Z. Zou, W. Hu, K. Wen, and H. Yang, *Chem. Eng. J.* 2019, **372**, 399-407.

18. C. Zachäus, F. F. Abdi, L. M. Peter, and R. Van De Krol, *Chem. Sci.* 2017, **8**, 3712-3719.

19. C. Ding, J. Shi, Z. Wang, and C. Li, *ACS Catal.* 2017, **7**, 675-688.

20. Z. Wang, X. Mao, P. Chen, M. Xiao, S. A. Monny, S. Wang, M. Konarova, A. Du, L. Wang, *Angew. Chem. Int. Ed.* 2019, **58**, 1030-1034.

21. F. Amano, M. Nakata, A. Yamamoto, T. Tanaka, *J. Phys. Chem. C* 2016, **120**, 6467-6474.

22. V. Donchev, T. Ivanov, K. Germanova, K. Kirilov, *Trends. Appl. Spectrosc*. 2010, **8**, 27−66